



Nanocrystalline β -Ti alloy with high hardness, low Young's modulus and excellent in vitro biocompatibility for biomedical applications



Kelvin Y. Xie ^{a,b,c}, Yanbo Wang ^{b,*}, Yonghao Zhao ^d, Li Chang ^b, Guocheng Wang ^b, Zibin Chen ^b, Yang Cao ^b, Xiaozhou Liao ^{b,*}, Enrique J. Lavernia ^e, Ruslan Z. Valiev ^f, Babak Sarrafpour ^g, Hans Zoellner ^g, Simon P. Ringer ^{a,b}

^a Australian Centre for Microscopy and Microanalysis, The University of Sydney, Sydney, NSW 2006, Australia

^b School of Aerospace, Mechanical and Mechatronics Engineering, The University of Sydney, Sydney, NSW 2006, Australia

^c Department of Mechanical Engineering, Johns Hopkins University, Baltimore, MD 21218, USA

^d School of Materials Science and Engineering, Nanjing University of Science and Technology, Nanjing 210094, China

^e Department of Chemical Engineering & Materials Science, University of California, Davis, CA 95616, USA

^f Institute of Physics of Advanced Materials, Ufa State Aviation Technical University, K. Marksa 12, Ufa 450000, Russian Federation

^g The Cellular and Molecular Pathology Research Unit, Department of Oral Pathology and Oral Medicine, Faculty of Dentistry, The University of Sydney, Westmead Centre for Oral Health, Westmead Hospital, NSW 2145, Australia

ARTICLE INFO

Article history:

Received 4 January 2013

Received in revised form 28 February 2013

Accepted 22 April 2013

Available online 29 April 2013

Keywords:

Ti alloy

High-pressure torsion

Mechanical properties

Cell attachment and proliferation

ABSTRACT

High strength, low Young's modulus and good biocompatibility are desirable but difficult to simultaneously achieve in metallic implant materials for load bearing applications, and these impose significant challenges in material design. Here we report that a nano-grained β -Ti alloy prepared by high-pressure torsion exhibits remarkable mechanical and biological properties. The hardness and modulus of the nano-grained Ti alloy were respectively 23% higher and 34% lower than those of its coarse-grained counterpart. Fibroblast cell attachment and proliferation were enhanced, demonstrating good in vitro biocompatibility of the nano-grained Ti alloy, consistent with demonstrated increased nano-roughness on the nano-grained Ti alloy. Results suggest that the nano-grained β -Ti alloy may have significant application as an implant material in dental and orthopedic applications.

© 2013 Elsevier B.V. All rights reserved.

1. Introduction

Pure Ti and Ti alloys are attractive materials for biomedical applications due to their light weight, high strength, relatively low Young's modulus and good biocompatibility. Currently Ti–6Al–4V (Ti64) is the most widely used commercial Ti alloy for dental and orthopedic applications [1–3]. Ti64 consists of both hexagonal close-packed α and body-centered cubic β phases, with a Young's modulus of ~110 GPa. Although Ti64 exhibits only half the Young's modulus of either stainless steel or Co–Cr alloys, it is still about 4 times stiffer than cortical bone (20–30 GPa) [1,4–6]. The difference in the modulus between artificial biomedical alloys and cortical bone creates a 'stress shielding' effect that undermines normal bone remodeling and maintenance and results in low bone density, loosening of implants, implant failure, and an increased likelihood for revision surgery [1,7]. Furthermore, the passive film of Ti64 can slowly leach-out toxic V ions [8], which have been linked to lower in-vitro cultured cell viability compared with pure Ti [9]. Therefore, the current research sought to

design a new generation of Ti alloys that has similar strength, but lower Young's modulus and better biocompatibility than Ti64.

Ti alloys consisting of mainly the β phase have recently drawn substantial attention because they exhibit Young's moduli ranging between 55 GPa and 90 GPa, and thus result in less stress shielding [9–13]. In addition, these Ti alloys contain only non-toxic elements such as Nb, Zr, and Ta [9,10,14], from which improved biocompatibility would be expected. Unlike Ti64 where V can leach out from the surface passive oxide film, the addition of Nb stabilizes the film, thus improving the passivation and corrosion resistance of Ti alloys in the body. Although high hardness and low Young's modulus are desirable qualities, they rarely coexist in this group of materials. This is because the single phase β -Ti alloys, which exhibit the lowest Young's modulus, are generally obtained after solution treatment, and so are relatively soft. Substantial strengthening can be achieved by aging treatments that induce a fine and uniform precipitation of ω and α phase components, but this inevitably increases the Young's modulus of the alloy [9,10,15,16]. Consequently, there is a critical need to devise strategies to produce β -Ti alloys that exhibit low Young's modulus, and high strength, and are thus more suitable for use in dental and orthopedic applications.

In this study, we demonstrate that it is possible to produce high strength of β -Ti alloys without long-time aging treatment, by reducing

* Corresponding authors.

E-mail addresses: yanbo.wang@sydney.edu.au (Y. Wang), xiaozhou.liao@sydney.edu.au (X. Liao).

the grain size of the material to the nanometer range using high-pressure torsion [17,18], and that this is achieved without a concomitant increase in Young's modulus. The nanocrystalline β -Ti alloy prepared in our studies displayed attractive mechanical properties, such that the hardness and Young's modulus of the nano-grained Ti alloy are respectively 23% higher and 34% lower than those of the coarse-grained counterpart. Furthermore, we demonstrated that the nanocrystalline β -Ti has increased surface nano-roughness, considered a plausible explanation for enhanced in vitro biocompatibility.

2. Experimental approach

The coarse-grained Ti alloy (Ti–36Nb–2.2Ta–3.7Zr–0.30 (at.)) was produced by arc melting and extruded into a long cylinder with a diameter of ~ 20 mm. Disks with a thickness of ~ 1.7 mm were sliced and then processed using high pressure torsion for 10 revolutions under 6 GPa at room temperature to obtain the nanocrystalline Ti alloy. Hardness tests were carried out from the center to the edges of specimens along radial directions on the disks using a Leco LV700AT hardness tester under a load of 10 kg with 15 s dwell time. Nanoindentation was performed using a Hysitron TriboIndenter under a load of 10 mN with a loading/unloading time of 10 s and dwell time 5 s.

Samples for transmission electron microscopy (TEM) investigation were ground and polished down to ~ 100 μm thickness, punched into 3 mm diameter disks and then electropolished using 8 vol.% H_2SO_4 in methanol at -40 $^\circ\text{C}$. In order to study the nature of the oxide forming on the coarse-grained and nanocrystalline Ti surfaces, cross sectional samples were also prepared. Ti alloys were mechanically polished to a mirror-like surface in 1 μm and then 200 nm colloidal silica suspension solutions at the final polishing step. Strips of materials were cut from the disks and the mirror-like surfaces were glued together. Specimens were then placed on a tripod such that the mirror-like surfaces were perpendicular to the grinding plane and mechanically ground and polished on a series of diamond lapping papers. The cross-sectional TEM specimens were attached to Cu rings and finally thinned down to electron transparency by ion milling at an incident angle of 6° using 4 keV argon ions at -20 $^\circ\text{C}$. Structural characterization was performed on a JEOL 3000F TEM operating at 300 kV.

For atomic force microscopy (AFM) and in vitro cell attachment/proliferation tests, coarse-grained and nanocrystalline Ti were mechanically polished to a mirror-like surface in the way described above. Ethanol was used to rinse away any residual colloidal silica. Surface tomography of the polished samples was evaluated by an AFM (PicoSPM) in tapping mode and four 5×5 μm^2 areas were scanned for each specimen.

Human gingival fibroblasts (HGF, passages 5–6, 8–9) and human dental follicular cells (HDfC, passages 4–5) were used to evaluate the in vitro biocompatibility of coarse-grained-Ti and the nanocrystalline β -Ti alloy. Mirror-like surface β -Ti alloy substrates were sterilized in 70% ethanol and under ultraviolet light for 20 min. Triplet cultures were made for each β -Ti alloy specimen in 6-well culture plates. Cells were then seeded and cultured in M199 with 10% bovine calf serum with antibiotics penicillin (100 U/ml), streptomycin (100 $\mu\text{g}/\text{ml}$) and amphotericin B (2.5 $\mu\text{g}/\text{ml}$), and incubated at 37 $^\circ\text{C}$, 5% CO_2 with 100% relative humidity. Control experiments were conducted on the coarse-grained β -Ti alloy in conventional tissue culture plates. For the cell attachment test, HGF were seeded at a density of 14,000 cells/ cm^2 and cultured for 30 min. For the cell proliferation tests, HGF and HDfC were seeded at a density of 4800 cells/ cm^2 and 2000 cells/ cm^2 , and cultured for 5 and 9 days respectively, changing medium every 3 days. For scanning electron microscopy (SEM) observations, cells were rinsed with phosphate-buffered solution, fixed with 2% glutaraldehyde and 1% osmium, and then dehydrated in graded alcohols and finally subjected to critical point drying. Samples were coated with 10 nm gold film and

subsequently observed using a field emission SEM (Zeiss Ultra). For fluorescent microscopy observations, cells were rinsed with PBS, fixed with 4% paraformaldehyde and stained using DAPI and phalloidin. Samples were observed under a reflective fluorescent microscope (Olympus BX61). The number of attached cell was counted in 4 randomly selected areas (1.5 mm^2 each) for each specimen. ANOVA and one tail t-tests were performed, with $p < 0.05$ considered statistically significant.

3. Results

Fig. 1a shows a typical bright-field TEM image of the as-extruded coarse-grained Ti alloy. The average grain size of the coarse-grained-Ti alloy was ~ 2 μm . Inset in Fig. 1a is a corresponding $\langle 110 \rangle_\beta$ zone axis selected area electron diffraction (SAED) pattern. The strong diffraction spots in the SAED pattern arise mainly from the β -Ti phase, while the weak diffuse diffraction spots (circled, Fig. 1a) are from the ω -Ti phase, indicating the co-existence of these two phases [19,20]. Fig. 1b shows a dark-field TEM image obtained using the circled diffraction spot in Fig. 1a, demonstrating that the ω phase (the bright areas in the figure) presents in the material as very fine precipitates distributed uniformly throughout the β phase matrix. Severe plastic deformation during high pressure torsion processing assists the formation of a nanocrystalline microstructure and the average grain size of the material was reduced to ~ 10 nm (Fig. 1c). A typical SAED pattern obtained from the nanocrystalline Ti alloy (Fig. 1d) reveals diffraction rings exclusively from the β -Ti phase (solid arrows). The dashed arrows indicate the positions for diffraction rings from the ω phase: the absence of diffraction rings at these positions indicates that the ω phase is absent in the nanocrystalline Ti alloy. Details on the high pressure torsion-induced phase evolution of the alloy have been reported elsewhere [21]. Fig. 2 shows the TEM images of both coarse-grained and nanocrystalline Ti samples in cross sectional view, revealing the nature of the oxide layer on mirror-like polished surfaces. An amorphous oxide layer with a thickness of 3–4 nm has developed on both samples with no crystalline form of oxides observed. Regular linear atomic arrays are seen in the coarse-grained material as opposed to disrupted arrays of atoms in nanocrystalline Ti as expected.

The roughness of the mirror-like polished surfaces of both coarse-grained and nanocrystalline Ti alloys was measured by AFM and results with corresponding Fourier modulus density diagrams are presented in Fig. 3. Scan areas of $\sim 1 \times 1$ μm^2 were cropped from larger scan areas (5×5 μm^2) to more clearly illustrate surface nano-roughness. From visual inspection, the coarse-grained Ti alloy (Fig. 3a) has a less rough surface compared to the nanocrystalline counterpart (Fig. 3b), although both specimens were polished in an identical way to achieve mirror-like surfaces. Surface roughness was also investigated quantitatively by comparing the corresponding Fourier modulus density diagrams of both surfaces. There is a hump (marked by the black arrow) present in the Fourier modulus density diagram in the nanocrystalline Ti in the range of 0.04–0.08 nm^{-1} in reciprocal space, indicating that the surface of nanocrystalline Ti has a large number of nano-crests/troughs 12.5–25 nm apart in real space. This however was not a prevalent feature on the coarse-grained Ti surface. Although there was a minor peak at 0.04 nm^{-1} (25 nm in real space) observed in the coarse-grained Ti Fourier modulus density diagram, it was much less prominent compared to the nanocrystalline Ti surface. It is also noteworthy that the surface roughness on coarse-grained and nanocrystalline Ti differs in frequency but not in magnitude. Multiple lines were drawn across AFM micrographs and the magnitude of surface roughness was measured to be $\sim \pm 2$ nm for both surfaces.

Hardness values were obtained by micro-indentation testing. The nanocrystalline β -Ti alloy reached 320 ± 6.2 Vicker's hardness (HV), compared to $\sim 260 \pm 5.2$ HV from the as-extruded coarse-grained material. The Young's moduli of both materials were measured using a nano-indentation test. Fig. 4 depicts typical nanoindentation

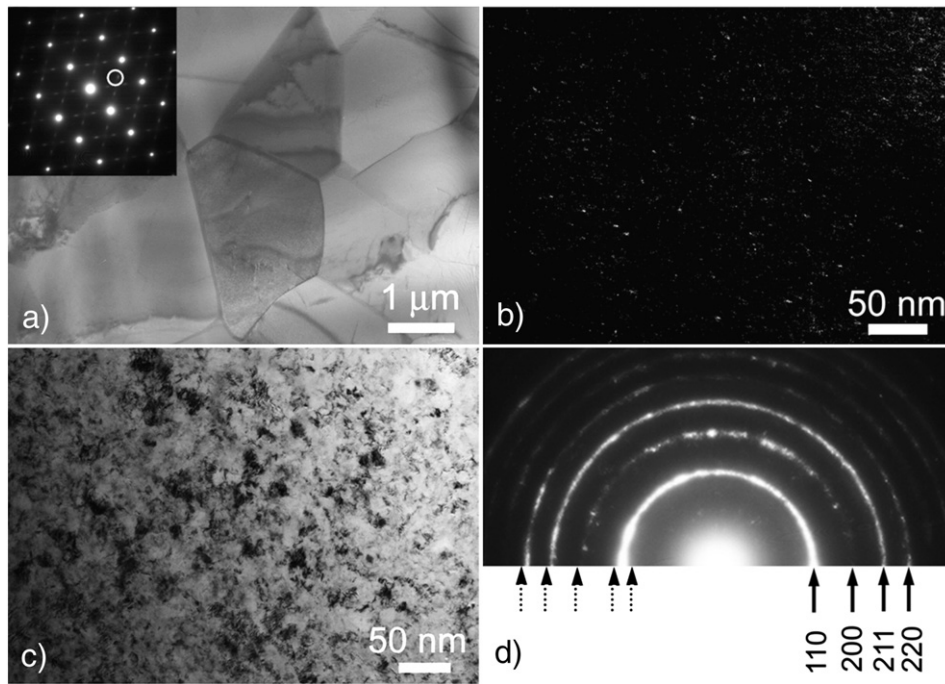


Fig. 1. (a) A typical bright-field TEM image and a selected area electron diffraction pattern for the as-extruded coarse-grained Ti alloy. (b) A typical dark-field TEM image using the circled diffraction spot in (a), showing the dispersion of fine ω phase precipitates in the β -Ti matrix. (c) A bright-field TEM image and (d) selected area electron diffraction pattern of the nanocrystalline β -Ti alloy. Solid arrows indicate diffraction from β -Ti. Dashed arrows mark the diffraction positions of the ω phase and confirm the absence of the ω phase.

load-displacement curves of the coarse-grained and nanocrystalline Ti alloy. A load of 10 μ N was used on both coarse-grained and nanocrystalline Ti alloys. The absolute displacement value of the indenter tip into nanocrystalline Ti was smaller than that of coarse-grained Ti, indicating a greater hardness for the nanocrystalline Ti material. To facilitate direct comparison, the relative displacement, which is represented by the actual displacement of the tip from the initial contact of the specimen surface (Δd) over the maximum displacement of the tip from the initial contact of the specimen surface into the material (d), was used in Fig. 4 to describe displacement rather than absolute displacement. During the unloading process, it is obvious that the elastic restoration is more prominent in the nanocrystalline Ti than in the coarse-grained Ti, consistent with a lower Young's modulus in nanocrystalline Ti. Measurement of the Young's modulus confirmed a lower value for the nanocrystalline β -Ti alloy of only 43.3 ± 0.4 GPa compared to 65 ± 0.5 GPa in the coarse-grained Ti alloy.

Along with the combination of high hardness and low Young's modulus, the nanocrystalline β -Ti also exhibited excellent in vitro biocompatibility as demonstrated via cell attachment and cell proliferation tests. The SEM images illustrate that HGF attached to both the coarse-

grained Ti alloy (Fig. 5a) and nanocrystalline β -Ti alloy specimen (Fig. 5b) surfaces after 30 min of attachment time. Some of the attached cells also had morphology indicative of cell spreading, as indicated in the insets in Fig. 5a–b. The histogram in Fig. 5c shows the HGF density on routine plastic culture plate surfaces, coarse-grained and nanocrystalline β Ti alloy. The number of HGF attached to the nanocrystalline β -Ti phase was significantly higher ($p < 0.05$) than that on the coarse-grained Ti. Fig. 6a–b further demonstrates that by 5 days of culture, the HGF had fully spread out on both the coarse-grained Ti alloy and the nanocrystalline β -Ti alloy surfaces. Here, the cells exhibited the characteristic fusiform fibroblast morphology including extensive filopodia, consistent with strong cell adhesion and growth on the β -Ti alloys. The density of HGF on coarse-grained Ti was similar to that of control HGF cultured on tissue culture plastic, consistent with the absence of any clear toxic activity in our β -Ti alloy. There was significantly more HGF proliferation on the nanocrystalline β -Ti surface compared to the control and coarse-grained Ti ($p < 0.05$) as shown in Fig. 6c, with ~40% higher HGF density on the nanocrystalline β -Ti alloy surface, suggesting an excellent in vitro biocompatibility. Human dental follicular cells (HDFC) were also used in a separate cell proliferation test.

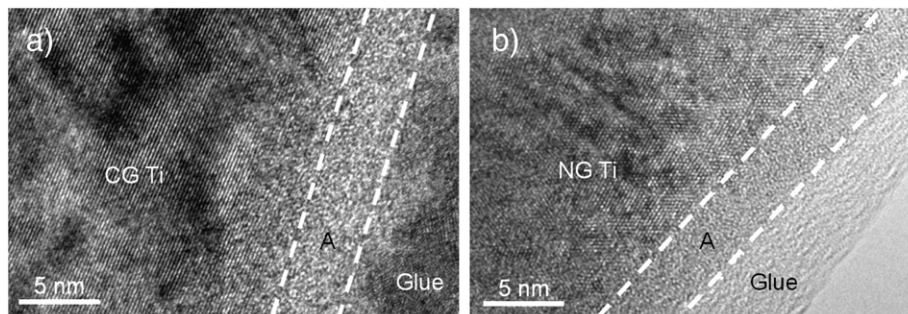


Fig. 2. Cross sectional TEM images of (a) coarse-grained Ti and (b) nanocrystalline Ti after polishing to mirror-like surface finish with amorphous oxide layer present. A: Amorphous layer.

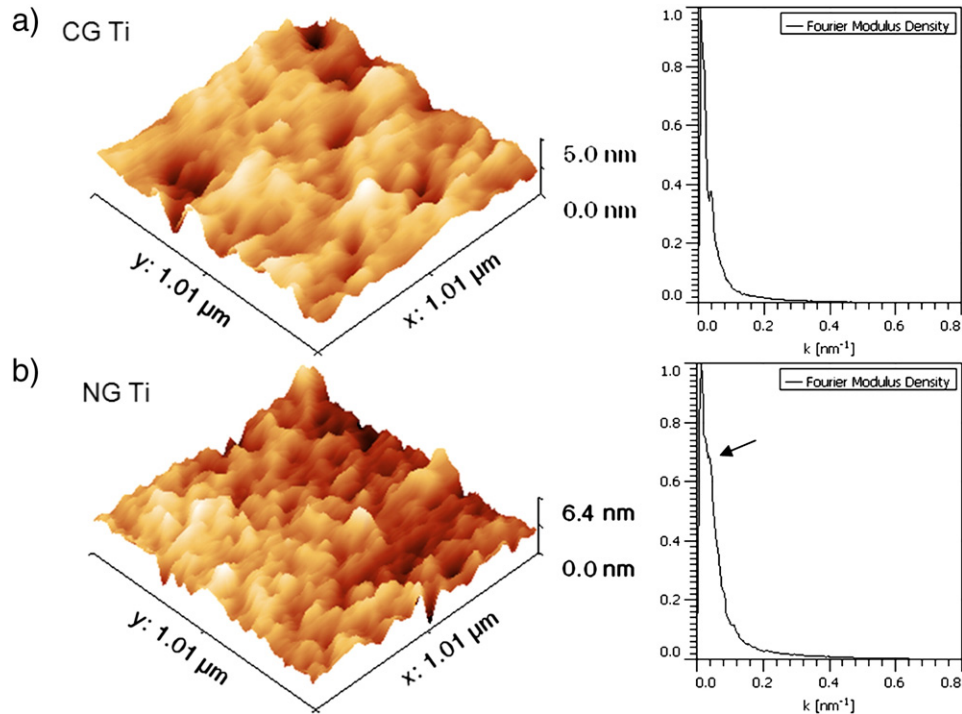


Fig. 3. AFM images of (a) CG and (b) nanocrystalline Ti alloy with corresponding Fourier modulus density diagrams in scan areas of $\sim 1 \times 1 \mu\text{m}^2$.

After 9 days of culturing, a significantly higher cell density ($p < 0.05$) was observed in the nanocrystalline β -Ti alloy, further indicating an enhanced in vitro biocompatibility.

4. Discussion

The mechanical properties, along with phase composition, of the coarse-grained-Ti alloy and the nanocrystalline β -Ti alloy investigated in this study as well as those of other Ti alloys commonly used for biomedical applications are summarized in Table 1. Nanocrystalline materials are known to be substantially harder than their coarse-grained counterparts due to the combined effect of high dislocation densities and small grain sizes [17,18]. In certain cases, good ductility is retained in nanocrystalline materials because of some unique deformation mechanisms operating in the nanocrystalline materials [22–25]. In this study, the nanocrystalline β -Ti alloy is $\sim 23\%$ harder than the as-extruded coarse-grained material. The grain refinement

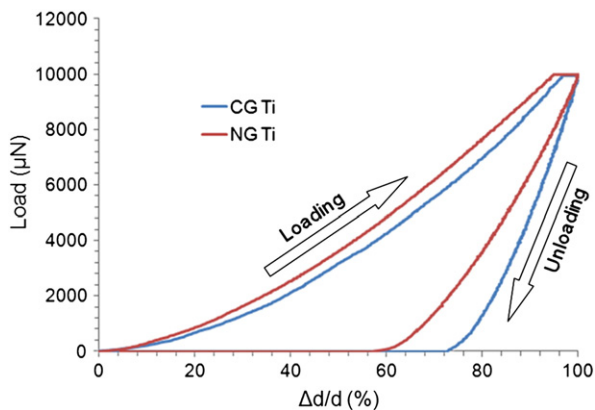


Fig. 4. The nanoindentation load-displacement curves of the coarse-grained and the nanocrystalline Ti alloy. Note that relative displacement is represented by using the actual displacement of the tip over the maximum displacement of the tip from the initial contact with the specimen surface ($\Delta d/d$).

significantly hardens the material as the grain size is reduced from $\sim 2 \mu\text{m}$ in the coarse-grained counterpart to $\sim 10 \text{ nm}$ in nanocrystalline β -Ti [26]. The nanocrystalline β -Ti also doubles the hardness of conventional commercial coarse-grained pure Ti ($\sim 160 \text{ HV}$) used for biomedical applications [27] and harder than most of the Ti alloys currently used in biomedical applications as shown in Table 1 [3,7,9,28].

The Young's modulus of the nanocrystalline β -Ti alloy was measured to be 34% lower than that in the as-received coarse-grained Ti alloy. This value (43.3 GPa) is even lower than the lowest Young's modulus of 55 GPa in the Ti alloys with similar chemical composition (Ti–35Nb–7Zr–5Ta) reported in the literature [1]. The low Young's modulus in the nanocrystalline β -Ti can be rationalized on the basis of two factors, being firstly the introduction of a significant amount of crystalline defects such as grain boundaries by high pressure torsion [29], and secondly the complete elimination of the ω phase from the β phase matrix [15,21]. In related studies, Akmadeev et al. demonstrated that severe plastic deformation (e.g., high pressure torsion) could effectively reduce the Young's modulus of a material. In their work, NG Cu exhibited a lower Young's modulus (115 GPa) than that of the coarse-grained Cu material studied (128 GPa) [29]. The reduction of Young's modulus in the nanocrystalline material can be explained by the substantial increase in the volume fraction of grain boundaries and grain boundaries' non-equilibrium structure introduced by high pressure torsion, since the Young's modulus near a grain boundary is lower than that in a perfect crystal [29]. Therefore, increasing the proportion of boundary regions effectively reduces the overall Young's modulus of the material in the nanocrystalline β Ti. Furthermore, the absence of ω phase in the nanocrystalline β Ti also contributes to its overall low Young's modulus. It has been known that the ω phase has much higher rigidity than the β phase and it has even greater effect on increasing the Young's modulus than the α phase in Ti alloys [1,16,19,30]. Interestingly, when the grain size of the alloy is refined down to $\sim 10 \text{ nm}$, the presence of the ω -phase is completely eliminated due to the ω -to- β transformation caused by grain size reduction into the nanocrystalline region [21]. Our as-extruded alloy was also designed to be a gum metal, which is a newly developed β -Ti alloys that exhibits unusual

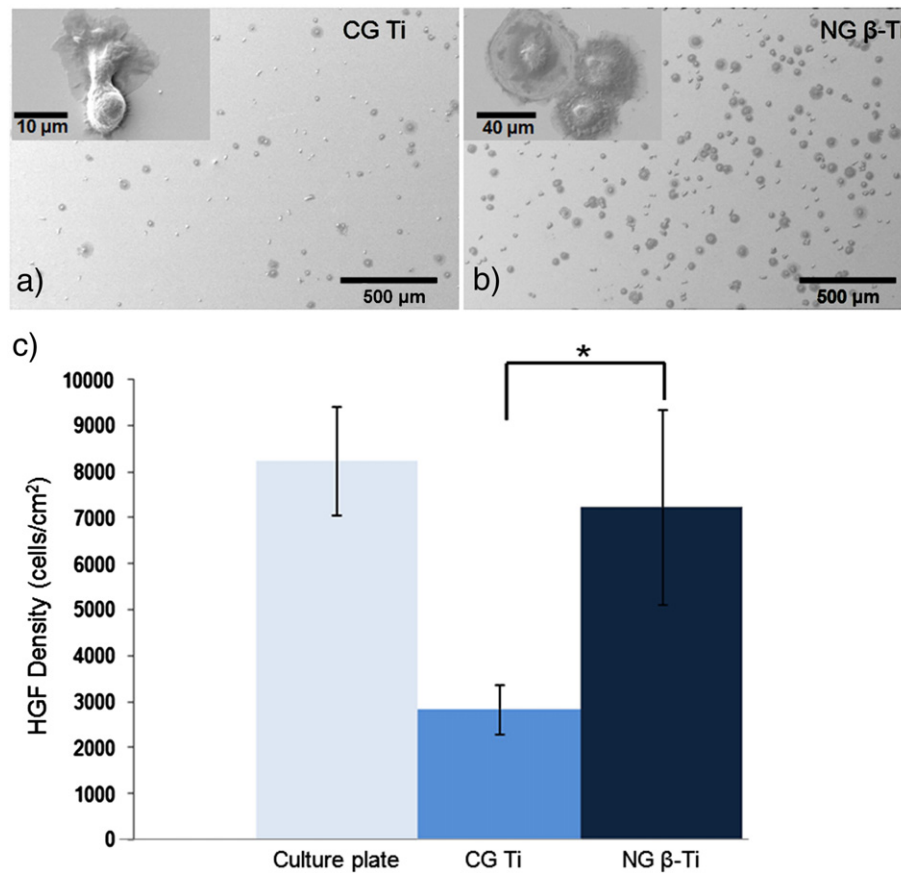


Fig. 5. Scanning electron microscopy images of human gingival fibroblasts (HGF) 30 min after cell seeding on (a) coarse-grained Ti and (b) nanocrystalline β -Ti evaluating the ability of cells to adhere to each surface tested. (c) Histogram showing HGF culture density on routine plastic culture plate surfaces, coarse-grained and nanocrystalline β -Ti alloy. The asterisk indicates the statistically significant difference ($p < 0.05$).

combinations of mechanical properties [31]. It has been reported that 90% cold-work on the as-annealed gum metal reduces its Young's modulus from ~65 to ~55 GPa at room temperature [31]. Similarly, high pressure torsion, a process that introduces much more severe plastic deformation than conventional cold-work, should also have a similar effect that lowers the Young's modulus of the nanocrystalline β -Ti.

One major advantage of our nanocrystalline β -Ti alloy is that it has a much lower Young's modulus than that of nanocrystalline pure α -Ti (Table 1). The low Young's modulus in nanocrystalline β -Ti is believed to enhance its in vivo biocompatibility when used in knee and hip prosthesis as compared to α -Ti. The Young's modulus of the nanocrystalline β -Ti alloy was measured to be only 43.3 ± 0.4 GPa, which so far is the lowest Young's modulus reported in metallic biomaterials and the closest to that of human cortical bone (20–30 GPa) [1,4–6]. The high value of the Young's modulus in the implant material results in stress shielding in load bearing biomedical applications and subsequently leads to bone resorption around implant material. Furthermore, in vivo studies carried out by Niinomi et al. on rabbits with experimental tibial fractures showed that implant materials with a high Young's modulus retarded the healing process, and induced early atrophy of the posterior proximal tibial bone [10]. Therefore, it seems highly desirable to achieve a value of Young's modulus that is close to that of bone in the nanocrystalline β -Ti.

Furthermore, nano-size features such as nano-grains, nano-fibers and nano-tubes have been known to modulate cell-material interaction [32–38]. The observed enhancement of cell attachment and proliferation may be attributed to the nanocrystalline characteristics of the crystallinity

β -Ti. Our work is in good agreement with that of Faghihi et al. [33,34] and Khang et al. [39], who also reported significantly improved pre-osteoblast and endothelial cell attachment, proliferation and viability on nanocrystalline pure α -Ti compared with coarse-grained α -Ti and control culture plastic plates. Two possible explanations have been postulated to understand the enhanced cell-substrate interaction on nanocrystalline Ti surface. The first possible explanation is that the oxide layers to which cells attach are different between nanocrystalline and coarse-grained Ti surfaces. Faghihi et al. reported that rutile structure of titanium oxide was observed on nanocrystalline Ti surface but not on coarse-grained counterparts [33,34]. They corroborated the increased surface wettability and cell-substrate interaction on nanocrystalline Ti surface with the difference in the oxides. The second possible explanation is that nanocrystalline materials obtained via severe plastic deformation store some of the strain energy from the deformation process, and that during polishing, the grains at the surface readily release the energy to create nano-roughness. In this study and as shown in Fig. 2, oxide layers on both nanocrystalline and coarse-grained Ti were amorphous and there was no obvious difference in the oxide layers as observed in cross-sectional TEM. Therefore, the observed enhanced cell-nanocrystalline Ti interaction is unlikely related to any differences in the nature of the surface oxide layers on β -Ti. The difference between our observation and work reported by Faghihi et al. is possibly attributable to the differences in the materials studied; BCC β -Ti was used as the substrate in this study whereas HCP pure α -Ti was used in theirs. The enhanced cell attachment and proliferation thus can be explained by the increased nano-roughness on the nanocrystalline Ti surface. Our AFM results reveal that although the nano-roughness on both coarse-grained and

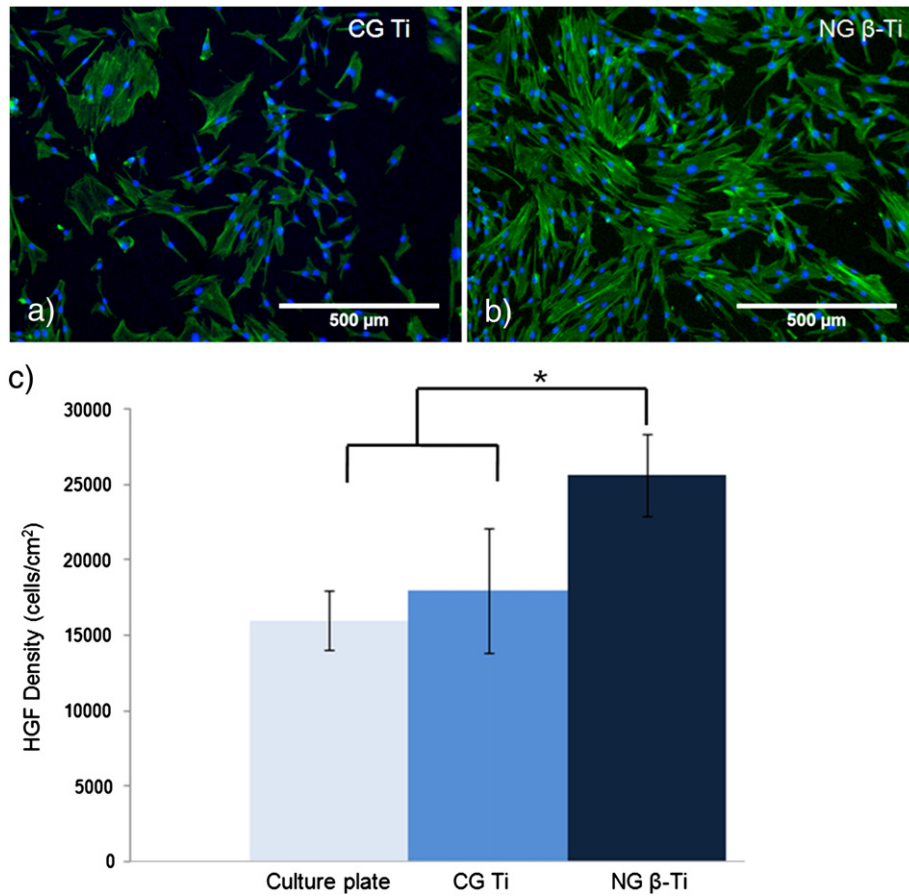


Fig. 6. Fluorescent images of HGF cultured for 5 days on (a) coarse-grained and (b) nanocrystalline β-Ti. (c) Histogram showing HGF density on routine plastic culture plate surfaces, coarse-grained and nanocrystalline β-Ti alloy. Data indicate greater proliferation of HGF on the nanocrystalline β-Ti surface relative to other surfaces tested, consistent with improved biocompatibility. The asterisk indicates the statistically significant difference ($p < 0.05$).

nanocrystalline Ti surfaces had very similar magnitudes ($\sim \pm 2$ nm), the frequency was much higher on the nanocrystalline Ti surface as shown in Fig. 3. It was also noticed that most of the nano-crests/troughs were 12.5–25 nm apart and that this scale was comparable to the average grain size of ~ 10 nm in the nanocrystalline Ti. Although both the coarse-grained and nanocrystalline β-Ti were polished to mirror-like surfaces in this study, nanocrystalline Ti has a larger surface area and surface energy than coarse-grained Ti, consistent with increased potential for interaction with cells that ultimately leads to enhanced cell attachment and proliferation on nanocrystalline Ti alloys [34,39].

It is noteworthy that the nanocrystalline β-Ti alloy not only has superior in vitro biocompatibility compared to its coarse-grained counterpart, the cell density on nanocrystalline Ti is also significantly

higher than that on the culture plate after 5-day culturing, as shown in Fig. 6c. It suggests that the nanocrystalline Ti surface is a more preferable substrate for cell proliferation than plastic substrate that is intentionally designed for cell culturing. This observation is in good agreement with the results reported by Faghihi et al. [34] that higher osteoblast and fibroblast density was observed on their NC α-Ti than that on a culture plate. The improved cell proliferation on the NG β-Ti alloy in this study can also be attributed to the enhanced nano-roughness on the nanocrystalline Ti surface while the plastic culture plate has a relatively flat surface.

5. Conclusions

The results of this study suggest that it is possible to design nanocrystalline β-Ti alloy that meets the simultaneous requirements of high strength, low modulus of elasticity and excellent biocompatibility. Notably, all of the alloying elements (Nb, Ta, Zr, and O) in the β-Ti alloy are non-toxic and non-allergic [9]. The nano-grain nature of the material concurrently leads to improved mechanical properties, nanotopography on the surface and in vitro biological responses. Higher strength is evident by the superior hardness which arises from grain refinement [40]. Lower rigidity was achieved, which is attributed to the nanocrystalline structure and the complete elimination of the ω phase. In addition to these desirable mechanical properties, the nanocrystalline β-Ti alloy also displays excellent in vitro biocompatibility, indicated by enhanced cell attachment and proliferation. This novel nanocrystalline β-Ti alloy has significant potential as a new generation of implant material with significant promise in load bearing biomedical applications.

Table 1

Comparison of the phases and mechanical properties of the Ti alloy studied here before and after high pressure torsion processing, and other commonly used Ti based implant materials. CP: commercial pure, ST: solution treated, STA: aged at 598 K for 259.2 ks after solution treatment. The properties of the Ti alloy from this study are in *italics*.

Description	Phases	E (GPa)	HV
Ti64 [3]	$\alpha + \beta$	120	310
CP coarse-grained Ti [27]	α	110	160
Pure nanocrystalline Ti [28]	α	105	275
Ti–29Nb–13Ta–4.6Zr (ST) [9]	β	62	175
Ti–29Nb–13Ta–4.6Zr (STA) [9]	$\beta + \alpha + \omega$	98	390
<i>Coarse-grained Ti alloy</i>	$\beta + \omega$	65	260
<i>nanocrystalline Ti alloy</i>	β	43	320

Acknowledgments

The authors are grateful for scientific and technical support from the Australian Microscopy & Microanalysis Research Facility (ammmf.org.au) node at The University of Sydney. The authors would also like to thank Drs E. Kelly, S. Fok, Y. Su, K. Jane, D. Cheng, N. Gokoolparsadh and S. Moody for their assistance on cell related and AFM work. This research was financially supported by the Australian Research Council (Grant No. DP110103117) (Y.B.W.). Y.H. Zhao and E.J. Lavernia acknowledge support by the Office of Naval Research (N00014-12-1-0237) with Dr. L. Kabacoff as program officer. Y.H. Zhao acknowledges the financial support from the Nanjing University of Science and Technology (2011ZDJH01).

References

- [1] M. Geetha, A.K. Singh, R. Asokamani, A.K. Gogia, *Prog. Mater. Sci.* 54 (2009) 397–425.
- [2] K.L. Wapner, *Clin. Orthop. Relat. Res.* (1991) 12–20.
- [3] M. Nakai, M. Niinomi, T. Akahori, N. Ohtsu, H. Nishimura, H. Toda, H. Fukui, M. Ogawa, *Mater. Sci. Eng., A* 486 (2008) 193–201.
- [4] J.Y. Rho, T.Y. Tsui, G.M. Pharr, *Biomaterials* 18 (1997) 1325–1330.
- [5] C.H. Turner, J. Rho, Y. Takano, T.Y. Tsui, G.M. Pharr, *J. Biomech.* 32 (1999) 437–441.
- [6] T. Hoc, L. Henry, M. Verdier, D. Aubry, L. Sedel, A. Meunier, *Bone* 38 (2006) 466–474.
- [7] C.N. Elias, J.H.C. Lima, R. Valiev, M.A. Meyers, *JOM* 60 (2008) 46–49.
- [8] P.J. Aragon, S.F. Hulbert, *J. Biomed. Mater. Res.* 6 (1972) 155.
- [9] M. Niinomi, *Biomaterials* 24 (2003) 2673–2683.
- [10] M. Niinomi, *J. Mech. Behav. Biomed. Mater.* 1 (2008) 30–42.
- [11] D. Raabe, B. Sander, M. Friák, D. Ma, J. Neugebauer, *Acta Mater.* 55 (2007) 4475–4487.
- [12] Y.L. Hao, S.J. Li, S.Y. Sun, C.Y. Zheng, R. Yang, *Acta Biomater.* 3 (2007) 277–286.
- [13] F.Q. Hou, S.J. Li, Y.L. Hao, R. Yang, *Scr. Mater.* 63 (2010) 54–57.
- [14] T. Naganawa, Y. Ishihara, T. Iwata, A. Koide, M. Ohguchi, Y. Ohguchi, Y. Murase, H. Kamei, N. Sato, M. Mizuno, T. Noguchi, *J. Periodontol.* 75 (2004) 1701–1707.
- [15] W.F. Ho, *J. Med. Biol. Eng.* 28 (2008) 47–51.
- [16] N. Sakaguchi, N. Mitsuo, T. Akahori, T. Saito, T. Furuta, in: S.G. Kang, T. Kobayashi (Eds.), *Designing, Processing and Properties of Advanced Engineering Materials*, Pts 1 and 2, Trans Tech Publications Ltd, Zurich–Uetikon, 2004, pp. 1269–1272.
- [17] A.P. Zhilyaev, T.G. Langdon, *Prog. Mater. Sci.* 53 (2008) 893–979.
- [18] R.Z. Valiev, *Nat. Mater.* 3 (2004) 511–516.
- [19] T. Yano, Y. Murakami, D. Shindo, Y. Hayasaka, S. Kuramoto, *Scr. Mater.* 63 (2010) 536–539.
- [20] M. Tane, T. Nakano, S. Kuramoto, M. Hara, M. Niinomi, N. Takesue, T. Yano, H. Nakajima, *Acta Mater.* 59 (2011) 6975–6988.
- [21] Y.B. Wang, Y.H. Zhao, Q. Lian, X.Z. Liao, R.Z. Valiev, S.P. Ringer, Y.T. Zhu, E.J. Lavernia, *Scr. Mater.* 63 (2010) 613–616.
- [22] R.Z. Valiev, I.V. Alexandrov, Y.T. Zhu, T.C. Lowe, *J. Mater. Res.* 17 (2002) 5–8.
- [23] R.Z. Valiev, R.K. Islamgaliev, I.V. Alexandrov, *Prog. Mater. Sci.* 45 (2000) 103–189.
- [24] Y.H. Zhao, X.Z. Liao, S. Cheng, E. Ma, Y.T. Zhu, *Adv. Mater.* 18 (2006) 2280.
- [25] Y.H. Zhao, J.E. Bingert, X.Z. Liao, B.Z. Cui, K. Han, A.V. Sergueeva, A.K. Mukherjee, R.Z. Valiev, T.G. Langdon, Y.T.T. Zhu, *Adv. Mater.* 18 (2006) 2949.
- [26] D.W. Callister, *Materials Science and Engineering: An Introduction*, John Wiley & Sons, Inc., York, 2007. 212–215.
- [27] L. Saldana, A. Mendez-Vilas, L. Jiang, M. Multigner, J.L. Gonzalez-Carrasco, M.T. Perez-Prado, M.L. Gonzalez-Martin, L. Munuera, N. Vilaboa, *Biomaterials* 28 (2007) 4343–4354.
- [28] A.V. Sergueeva, V.V. Stolyarov, R.Z. Valiev, A.K. Mukherjee, *Scr. Mater.* 45 (2001) 747–752.
- [29] N.A. Akhmadeev, N.P. Kobelev, R.R. Mulyukov, Y.M. Soifer, R.Z. Valiev, *Acta Metall. Mater.* 41 (1993) 1041–1046.
- [30] T. Yano, Y. Murakami, D. Shindo, S. Kuramoto, *Acta Mater.* 57 (2009) 628–633.
- [31] T. Saito, T. Furuta, J.-H. Hwang, S. Kuramoto, K. Nishino, N. Suzuki, R. Chen, A. Yamada, K. Ito, Y. Seno, T. Nonaka, H. Ikehata, N. Nagasako, C. Iwamoto, Y. Ikuhara, T. Sakuma, *Science* 300 (2003) 464–467.
- [32] S.L. Wu, X.M. Liu, T. Hu, P.K. Chu, J.P.Y. Ho, Y.L. Chan, K.W.K. Yeung, C.L. Chu, T.F. Hung, K.F. Huo, C.Y. Chung, W.W. Lu, K.M.C. Cheung, K.D.K. Luk, *Nano Lett.* 8 (2008) 3803–3808.
- [33] S. Faghihi, F. Azari, A.P. Zhilyaev, J.A. Szpunar, H. Vali, M. Tabrizian, *Biomaterials* 28 (2007) 3887–3895.
- [34] S. Faghihi, A.P. Zhilyaev, J.A. Szpunar, F. Azari, H. Vali, M. Tabrizian, *Adv. Mater.* 19 (2007) 1069–1073.
- [35] J. Park, S. Bauer, P. Schmuki, K. von der Mark, *Nano Lett.* 9 (2009) 3157–3164.
- [36] E. Mooney, P. Dockery, U. Greiser, M. Murphy, V. Barron, *Nano Lett.* 8 (2008) 2137–2143.
- [37] L.P. Zanello, B. Zhao, H. Hu, R.C. Haddon, *Nano Lett.* 6 (2006) 562–567.
- [38] C.T. Wu, Y.F. Zhang, X.B. Ke, Y.X. Xie, H.Y. Zhu, R. Crawford, Y. Xiao, *J. Biomed. Mater. Res. Part A* 95A (2010) 476–485.
- [39] D. Khang, J. Lu, C. Yao, K.M. Haberstroh, T.J. Webster, *Biomaterials* 29 (2008) 970–983.
- [40] P.V. Liddicoat, X.Z. Liao, Y.H. Zhao, Y.T. Zhu, M.Y. Murashkin, E.J. Lavernia, R.Z. Valiev, S.P. Ringer, *Nat. Commun.* 1 (2010).